

# Configuration-interaction approach to nuclear fission

G.F. Bertsch<sup>1</sup> and K. Hagino<sup>2</sup>

<sup>1</sup> *Department of Physics and Institute of Nuclear Theory, Box 351560,  
University of Washington, Seattle, Washington 98195, USA*

<sup>2</sup> *Department of Physics, Kyoto University, Kyoto 606-8502, Japan*

We propose a configuration-interaction (CI) representation to calculate induced nuclear fission with explicit inclusion of nucleon-nucleon interactions in the Hamiltonian. The framework is designed for easy modeling of schematic interactions but still permits a straightforward extension to realistic ones. As a first application, the model is applied to branching ratios between fission and capture in the decay modes of excited fissile nuclei. The ratios are compared with the Bohr-Wheeler transition-state theory to explore its domain of validity. The Bohr-Wheeler theory assumes that the rates are insensitive to the final-state scission dynamics; the insensitivity is rather easily achieved in the CI parameterizations. The CI modeling is also capable of reproducing the branching ratios of the transition-state hypothesis which is one of the key ingredients in the present-day theory of induced fission.

*Introduction.* The theory of induced fission is one of the most challenging subjects in many-fermion quantum dynamics. In a recent review [1] of future directions in fission theory, the authors omitted the topic “because there has been virtually no coherent microscopic theory addressing this question up to now.”

In this Letter we propose a microscopic approach based on many-body Hamiltonians in the configuration-interaction (CI) framework. The idea is not new [2], but the methodology has yet to be applied in practice<sup>1</sup>. Before realistic calculations can be contemplated, it is useful to consider simplified models in the many-particle framework that are extensible to the realistic domain [5–7]. Such models may validate the phenomenological approaches that have been with us since the beginnings of fission theory, or it may suggest modifications to them. The focus here is on how the system crosses the fission barrier; key observables are the excitation function for fission cross sections and the branching ratio between fission and other decay channels. The model proposed below incorporates microscopic mechanisms to propagate the systems from the initial ground-state shape to a region beyond the fission barriers(s).

*Hamiltonian.* We build the Hamiltonian on a set of reference states  $Q$ , each such state generating a spectrum of quasiparticle excitations which we call a  $Q$ -block. The  $Q$ -blocks are ordered by deformation  $Q_2$ . The Hamiltonian is constructed from these elements as

$$\hat{H} = \sum_Q \left( E_{\text{gs}}(Q) + \hat{H}_{\text{qp}}(Q) + \hat{H}_v(Q) + f_{\text{od}} \sum_{Q'=Q\pm 1} \hat{H}_v^{\text{od}} \right). \quad (1)$$

Here  $E_{\text{gs}}$  is the energy of the reference state, calculated by constrained Hartree-Fock or density functional the-

ory<sup>2</sup> (DFT). In the model below we choose appropriate sets of energies  $E_{\text{gs}}(Q)$  to explore various limits of the theory. The circumflexes denote terms containing Fock-space operators acting within a  $Q$ -block or between orbitals in adjacent  $Q$ -blocks. We detail them below.

*Constructing the configurations.* The configuration space is built in the usual way, defining configurations as Slater determinants of nucleon orbitals. The orbitals are envisioned as eigenstates of an axially deformed single-particle potential. Ultimately their properties would be determined by the density functional theory, but for modeling purposes we found it convenient to assume a uniform spectrum of orbital energies with the same spacing  $d$  for protons and neutrons. The ladder of orbital states extends infinitely in both directions above and below the Fermi surface. The operator for the quasiparticle excitation energy  $E_{\text{qp}}$  is given by

$$\hat{H}_{\text{qp}} = d \sum_{\alpha: n_\alpha > 0} n_\alpha \hat{a}_\alpha^\dagger \hat{a}_\alpha + d \sum_{\alpha: n_\alpha \leq 0} n_\alpha \hat{a}_\alpha \hat{a}_\alpha^\dagger. \quad (2)$$

The label  $\alpha$  includes all quantum numbers associated with the orbital,  $\alpha = (Q, n, K, t)$ . Here  $n$  indexes the orbital position in the ladder, with  $n = 0$  corresponding to the Fermi level, and  $K$  is its angular momentum about the symmetry axis. To keep the model as transparent as possible, we restrict  $K$  to  $\pm 1/2$ . The label  $t$  distinguishes neutrons (n) and protons (p).

The orbital excitation energies of many-particle configurations are integral multiples of  $d$ ,  $E_{\text{qp}} = E_k = k d$ . As a function of  $k$ , the multiplicity of configurations having  $\sum K = 0$  is  $N_k = (1, 4, 16, 48, 133, 332, 784, \dots)$  for  $k = (0, 1, 2, 3, 4, 5, 6, \dots)$ . The spectrum up to  $k = 11$  is shown in Fig. 1. Its functional form agrees well with the leading behavior of the Fermi-gas level density formula [9] as described in the figure caption. The histogram shows

<sup>1</sup> There has been earlier work calculating the dynamics by a diffusion equation with a microscopic treatment of the diffusion coefficient [3, 4].

<sup>2</sup> We note that theory based on Hamiltonian interactions together with orbitals from DFT has been successfully applied elsewhere [8].

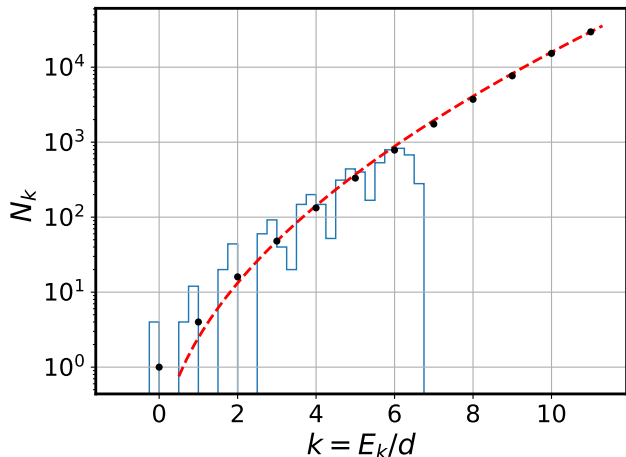


FIG. 1: Spectrum of many-body configurations in the uniform model. Here, the total  $K$  quantum number of the system is restricted to  $K = 0$ .  $N_k$  denotes the number of configurations at the excitation energy  $E^* = kd$ . The filled circles and the histogram show the non-interacting and the interacting spectra, respectively. The dotted red curve shows a fit to the functional form  $\log(N_k) \sim \sqrt{k}$ .

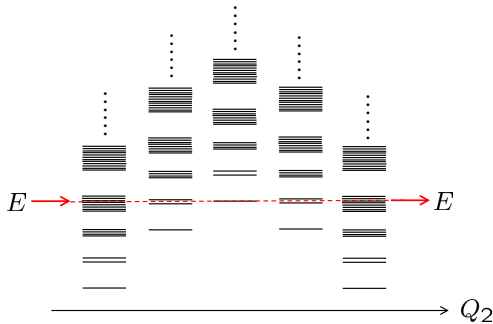


FIG. 2: The vertical towers of levels are the  $Q$ -blocks in the basis of configurations. They are ordered by deformation  $Q_2$ .  $E$  is the incident energy for a fission reaction.

the level density after including  $\hat{H}_v$  in the Hamiltonian of the  $Q$ -block.

The parameter  $d$  will be left unspecified below. It can vary greatly due to shell effects, but in the actinide nuclei it is in the range  $0.4 - 0.5$  MeV [33]. The levels at the neutron emission threshold would then correspond to  $k \approx 13 - 16$  in excitation energy and somewhat higher  $k \approx 17$  in level density. What we have described here is a single-reference basis of configurations. Fission requires large-amplitude shape changes, which cannot be reasonably treated in a single-reference basis. As a minimum, one needs to extend the space by including as reference states the local DFT minima across the saddle point of the barrier [10]. In fact there are many such minima along typical fission paths [11]. In our model we organize the reference configurations as a chain along a path of

increasing deformations, as depicted in Fig. 2. One complication at this point is that the resulting basis may not be orthogonal. We shall come back to this point later.

*Model nucleon-nucleon Hamiltonians.* In the quasiparticle representation, there are three kinds of two-particle interaction. The interactions that are diagonal in quasiparticle occupations factors are taken into account in  $E_{\text{gs}}$ , the ground state energy of the reference configuration. The interactions changing the orbital of one of the nucleons do not contribute in the reference configuration if it is a stationary state of the DFT; otherwise it induces a diabatic transformation of the configuration. Such transformations are generally unfavored on energetic grounds [12] and they are omitted in the present model. We are left with the interactions that change the orbitals of both particles. In this Letter we deal only with the neutron-proton interaction. The pairing interaction between identical particles is certainly important as well; in fact, it is likely to be more important in non-diabatic collective dynamics [7, 14]. However, it is also important to assess the effects of the residual neutron-proton interaction [3], and this has not been done until now.

We write the interaction Hamiltonian as

$$\hat{H}_v = v_{\text{np}} \sum' r \hat{a}_{\alpha_1}^\dagger \hat{a}_{\alpha_2}^\dagger \hat{a}_{\alpha_3} \hat{a}_{\alpha_4}. \quad (3)$$

where the parameter  $v_{\text{np}}$  is the strength of the interaction and  $r$  is a random variable from a Gaussian ensemble of unit variance. The summation is over the four  $\alpha$  indices restricted to a fixed  $Q$  in  $\hat{H}_v$  and to neighboring  $Q$ -blocks [3–7, 10] in  $\hat{H}_v^{\text{od}}$ . Also, the sum is restricted to  $\alpha$  sets satisfying  $K_1 + K_2 = K_3 + K_4$ . The assumption that the neutron-proton interaction is Gaussian distributed is certainly not justified for the low-energy states in a  $Q$ -block where collective excitations can be built up. However, high in the spectrum where only the overall interaction strength is important the mixing approaches the random matrix limit. The strength can be determined by sampling with more realistic interactions that could range in sophistication from simple contact interactions or separable interactions to those used in present-day shell model Hamiltonians. The strength of neutron-proton contact interactions for shell model Hamiltonians is typically in the range  $250 - 500$  MeV-fm<sup>3</sup> [3, 13]. The corresponding strength in actinides [33] for our parameterization is  $0.05d - 0.1d$ ; we take  $v_{\text{np}} = 0.05d$  in most of the examples below.

The configurations may be characterized by the number of quasiparticles as well as by the energy index  $k$ . Each  $k \neq 0$  subblock contains configurations going from two quasiparticles to the maximum energetically allowed. The subblocks are all connected by the residual interaction, although the matrices connecting them are sparse. For example, the  $N_6 \times N_6$  matrix has an off-diagonal filling of 5%, while the  $N_6 \times 1$  matrix connecting the  $k = 6$  subblock to the ground state is 27% filled.

In the presence of the residual interaction, the eigenstates of a shell-model configuration space are found to approach the random matrix limit of the Gaussian

Orthogonal Ensemble (GOE) when the rms interaction strength is larger than the level spacing between configurations [15, 16]. For reaction theory, the most important GOE characteristic is the Porter-Thomas distribution of decay widths, requiring a nearly Gaussian distribution of configuration amplitudes in the eigenstates. The eigenstates of large-dimension  $k$ -subblocks do in fact acquire the properties of the GOE, even though the sparseness of the interaction matrix works against a complete mixing of the configurations [33]. More realistic model that do not permit the  $k$  grouping will still approach the GOE at high excitation energy. However, it should be mentioned that a numerical study [17, 18] of a light-nucleus spectrum did not confirm the above stated criterion for GOE behavior.

The interaction between  $Q$ -blocks is responsible for shape changes [3] and is thus crucial to the modeling. It is clear that the interaction is somewhat suppressed due to the imperfect overlap of orbitals built on different mean-field reference states. Another complication is that the configurations in different  $Q$ -blocks will not be orthogonal unless special measures are taken, e.g., restriction by  $K$ -partitioning [19]. These problems have long been dealt with in other areas of physics [20–22] and can be treated in nuclear physics in the same way. For our model, we simply parameterize the effects by the attenuation factor  $f_{\text{od}}$  in Eq. (1).

*Reaction theory.* Induced fission is in the domain of reaction theory: an external probe, typically a neutron, excites the nucleus leading to its decay by fission. A number of reaction-theoretic formalisms are available for treating CI Hamiltonians. We mention in particular<sup>3</sup> the  $K$ -matrix formalism [5, 25–28] and the  $S$ -matrix formalism [24, 25]. The key quantity is the transmission coefficient from an incoming channel to the decay channels of interest,

$$T_{\text{in},C} = \sum_{j \in C} |S_{\text{in},j}|^2. \quad (4)$$

Here  $C$  is the set of quantum mechanical channels associated with the type of reaction. For neutron-induced reactions on heavy nuclei, it could be inelastic scattering, capture, or fission. The relevant  $S$ -matrix quantities may be calculated as [28, 29]

$$|S_{j,j'}|^2 = \sum_{\mu,\mu'} \Gamma_{j,\mu} |(\tilde{H} - E)^{-1}|_{\mu,\mu'}^2 \Gamma_{j',\mu'}. \quad (5)$$

Here  $\Gamma_{i,\mu}$  is the decay width of the state  $\mu$  into the channel  $i$ . Note that the CI Hamiltonian  $H$  is modified by including of the coupling to the channels. We assume

<sup>3</sup> Early studies also made use of the  $R$ -matrix theory [23–25]. However, it requires unphysical boundary conditions that are difficult to implement.

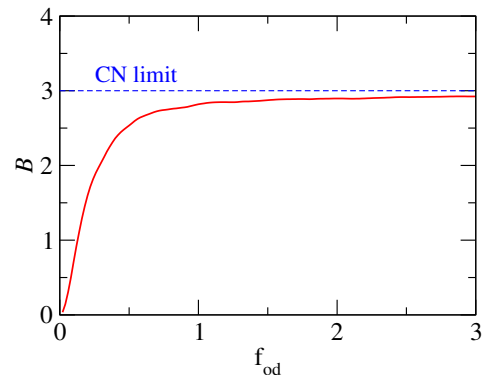


FIG. 3: The branching ratio as a function of the attenuation factor  $f_{\text{od}}$  in the interaction between  $Q$ -blocks. The model space is  $(k = 0 - 4) \times 3$  and the reference-state energies are  $E_{\text{gs}} = (0.0, 0.0, 0.0)$ . Other parameters are:  $v_{\text{np}} = 0.05d$ ,  $\Gamma_{\text{cap}} = 0.001d$ , and  $\Gamma_{\text{fis}} = 0.003d$ . The energy average in Eq. (7) is taken in the range of  $3.5d \leq E \leq 4.5d$ . The dashed line denotes the branching ratio in the compound nucleus limit,  $B_{\text{cap,fis}} = \Gamma_{\text{fis}}/\Gamma_{\text{cap}} = 3.0$ .

in the model that each channel couples to a single internal configuration, and we neglect dispersive effects. The modified Hamiltonian  $\tilde{H}$  then reads,

$$\tilde{H}_{\mu,\mu'} = H_{\mu,\mu'} - i\delta_{\mu,\mu'} \sum_j \Gamma_{j,\mu}/2. \quad (6)$$

The main observable we are interested in is the branching ratio between fission and capture. We define it as

$$B_{\text{cap,fis}} = \frac{\int dE T_{\text{in,fis}}}{\int dE T_{\text{in,cap}}}. \quad (7)$$

The range of integration is the same for numerator and denominator and in practice would be determined by experimental considerations. For simplicity, we assume that the entrance channel width is small compared to the decay widths, in which case it cancels out of Eq. (7). For a typical example the experimental quantities are  $\Gamma_{\text{cap}} \approx 0.04\text{eV}$  and  $B_{\text{cap,fis}} \approx 3$  [26].

*Results.* We can now set the parameters to simulate the branching between capture and fission processes. To this end, we consider chains of three or more  $Q$ -blocks; the first represents the spectrum built on the ground state and the last has the doorway state to fission channels. Imaginary energies  $-i\Gamma_{\text{cap}}/2$  and  $-i\Gamma_{\text{fis}}/2$  are added to the blocks in  $\tilde{H}$  to account for the decay widths [5].

As a warm-up, we find conditions on  $f_{\text{od}}$  that justify the compound-nucleus (CN) hypothesis that the relative decay rates are proportional to the decay widths in  $\tilde{H}$ . The model has three identical  $Q$ -blocks composed of  $k \leq 4$  subblocks. The calculated branching ratios are shown in Fig. 3. Note that the stochastic treatment of the interaction in Eq. (3) produces a distribution of ratios; only one of them is shown in the figure. For  $f_{\text{od}} \gtrsim 1$ , the branching ratio is consistent with the formula  $B_{\text{cap,fis}} =$

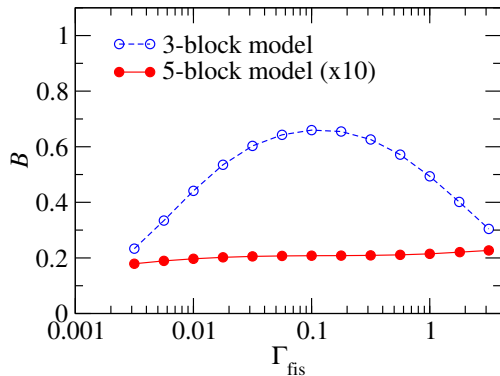


FIG. 4: Sensitivity of the branching ratio to the exit channel widths. The blue open circles are for the model space of  $(k = 0 - 6) \times 3$  with  $E_{\text{gs}} = (0, 6d, 0)$ , while the red filled circles are for  $(k = 0 - 6) \times 5$  with a parabolic barrier  $E_{\text{gs}} = (0.0, 4.5, 6.0, 4.5, 0.0)$ . Other parameters are:  $v_{\text{np}} = 0.05d$ ,  $f_{\text{od}} = 1.0$ , and  $\Gamma_{\text{cap}} = 0.01d$ . The incoming channel is assumed to be one of the configurations at  $E^* = 6d$  in the first block, and the energy average in Eq. (7) is taken in the range of  $5.5d \leq E \leq 6.5d$ .

$\Gamma_{\text{fis}}/\Gamma_{\text{cap}}$ , confirming the CN limit. Even with  $f_{\text{od}} = 0.5$ , the branching ratio is only 15% less than the CN limit.

We next impose a barrier and examine the fundamental assumption of present-day theory of induced fission, namely that near the barrier top the decay rate is by the Bohr-Wheeler (BW) transition state formula [30, 31]

$$\Gamma_{\text{BW}} = \frac{1}{2\pi\rho} \sum_i T_i. \quad (8)$$

Here  $i$  are states on the barrier top,  $T_i$  are transmission coefficients across the barrier, and  $\rho$  is the level density of the compound nucleus (i.e., the first  $Q$ -block) at the given excitation energy. Notice that the BW formula does not depend on the fission widths  $\Gamma_{\text{fis}}$ , unlike Eq. (5).

First consider the model space of 3 identical  $Q$ -blocks composed of  $k \leq 6$  subblocks, with  $E_{\text{gs}} = (0, 6d, 0)$  to make a barrier at the middle block. As may be seen in Fig. 4, this model fails the first assumption: the derived branching ratio is sensitive to the fission decay width,  $\Gamma_{\text{fis}}$ . The reason is that there are many virtual transitions possible through the higher levels in the barrier-top  $Q$ -block. Because the effective number of partially open channels is large, the communication between the end  $Q$ -blocks remains strong.

We found two ways to greatly diminish the dependence on  $\Gamma_{\text{fis}}$  in our model. The first way is to increase the chain of  $Q$ -blocks on the barrier. Then the path across the barrier requires multiple virtual transitions, resulting in a much stronger suppression factor. This may be seen in Fig. 4 for the 5-block case.

The other way is to eliminate the virtual transitions at the barrier by cutting off the spectrum of the middle block. Fig. 5 shows the results with 3  $Q$ -blocks. The first and the last blocks are defined as usual in the  $N_k$

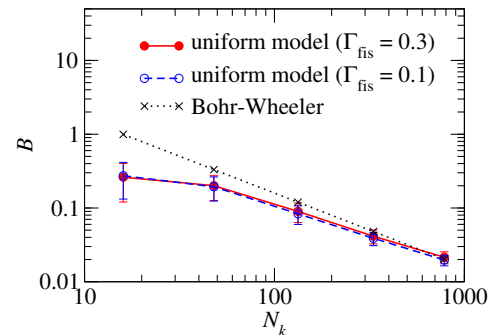


FIG. 5: Branching ratios in  $(k)/(0)/(k)$  configuration spaces in which the barrier  $Q$ -block is a single state degenerate with the other  $Q$ -blocks. Other parameters are  $v_{\text{np}} = 0.05d$ ,  $f_{\text{od}} = 1$  and  $\Gamma_{\text{cap}} = 0.01d$ . The filled circles and the open circles are obtained with  $\Gamma_{\text{fis}} = 0.3d$  and  $0.1d$ , respectively. The uncertainties are estimated with 100 different random number sets in the Hamiltonian matrix. The filled squares shows the predicted values from a schematic transition-state formula (see text for details).

space. The middle block has only a  $k = 0$  configuration, shifted in energy to  $E_{\text{qp}} = kd$ . The filled circles and the open circles show the branching ratios with  $\Gamma_{\text{fis}} = 0.3d$  and  $0.1d$ , respectively. There is hardly any difference between the two curves.

One can make a crude approximation to the Bohr-Wheeler transition state formula Eq. (8) within the framework of the model. The branching ratio for a single barrier state with a transmission factor  $T_i = 1$  reads  $B_{\text{cap,fis}} \sim 1/(2\pi\rho\Gamma_{\text{cap}})$ . The spread of the  $k$  subblock with the given parameters is about  $d$ , resulting in a level density  $\rho = N_k/d$ . This estimate gives the reasonable agreement shown by the filled squares in the Figure; it appears that the internal transmission factor for large spaces approaches  $T = 1$ . However, the comparison should not be considered quantitative because the level density of the first  $Q$ -block is not constant over the energy window accessed by the state in the middle.

*Summary and Outlook.* The model presented here for induced fission in a CI representation appears to be sufficiently detailed to examine the validity of transition-state theory in a microscopic framework. Depending on the interaction and the deformation-dependent configuration space, one achieves conditions in which branching ratios depend largely on barrier-top dynamics and are insensitive to properties closer to the scission point. The insensitive property is one of the main assumptions in the well-known Bohr-Wheeler formula for induced fission, but up to now it had no microscopic justification.

Whether the transition-state hypothesis is valid under realistic Hamiltonians remains to be seen and will require a large computational effort to answer. In the near term, the model can be applied in a number of different ways. We plan to study the barrier transmission factor

$T_i$  as a function of barrier height to test another basic assumption in present-day theory, namely treating them by the Hill-Wheeler formula [32, p. 1140]. It also appears quite straightforward to include a pairing interaction in the Hamiltonian. This would allow one to explore for

the first time the competition between the two kinds of interaction in barrier-crossing dynamics.

This work was supported in part by JSPS KAKENHI Grant Number JP19K03861.

- 
- [1] M. Bender *et al.*, J. Phys. G **47**, 113002 (2020).  
 [2] F. Dönau, J. Zhang and L. Riedinger, Nucl. Phys. **A496**, 333 (1989).  
 [3] B.W. Bush, G.F. Bertsch and B.A. Brown, Phys. Rev. **C45**, 1709 (1992).  
 [4] D. Cha and G.F. Bertsch, Phys. Rev. **C46**, 306 (1992).  
 [5] G.F. Bertsch, Phys. Rev. C **101**, 034617 (2020).  
 [6] K. Hagino and G.F. Bertsch, Phys. Rev. C **101**, 064317 (2020).  
 [7] K. Hagino and G.F. Bertsch, Phys. Rev. C **102**, 024316 (2020).  
 [8] D. Sangalli *et al.*, Phys. Rev. B **93**, 195205 (2016).  
 [9] A. Bohr and B.R. Mottelson, *Nuclear Structure* (W.A. Benjamin, Reading, MA, 1969), Vol. I.  
 [10] F. Barranco, G.F. Bertsch, R.A. Broglia, and E. Vigezzi, Nucl. Phys. **A512**, 253 (1990).  
 [11] G. F. Bertsch, W. Younes, and L. M. Robledo, Phys. Rev. C **100**, 024607 (2019).  
 [12] W. Nörenberg, Nucl. Phys. **A409**, 191 (1983).  
 [13] K. Yoshida, Prog. Theor. Exp. Phys. **2013**, 113D02 (2013).  
 [14] R. Rodríguez-Guzmán and L.M. Robledo, Phys. Rev. C **89**, 054310 (2014).  
 [15] T. Guhr and H.A. Weidenmüller, Ann. Phys. (N.Y.) **193**, 472 (1989).  
 [16] H.A. Weidenmüller and G.E. Mitchell, Rev. Mod. Phys. **81**, 539 (2009).  
 [17] B.A. Brown and G.F. Bertsch, Phys. Lett. B **148**, 5 (1984).  
 [18] V. Zelvinsky, B.A. Brown, N. Frazier, and M. Horoi, Phys. Rep. **276**, 85 (1996).  
 [19] G.F. Bertsch, Int. J. Mod. Phys. E **26**, 1740001 (2017).  
 [20] P.O. Löwdin, Phys. Rev. **97**, 1474 (1955).  
 [21] M.G. Reuter, T. Seideman, and M.A. Ratner, Phys. Rev. B **83**, 085412 (2011).  
 [22] J. Rodríguez-Laguna, L.M. Robledo, and J. Dukelsky, Phys. Rev. A **101**, 0125105 (2020).  
 [23] A.M. Lane and R.G. Thomas, Rev. Mod. Phys. **30**, 257 (1958).  
 [24] I.J. Thompson and F.M. Nunes, *Nuclear Reactions for Astrophysics* (Cambridge University Press, Cambridge, 2009).  
 [25] T. Kawano, P. Talou, and H.A. Weidenmüller, Phys. Rev. C **92**, 044617 (2015).  
 [26] G.F. Bertsch and T. Kawano, Phys. Rev. Lett. **119**, 222504 (2017).  
 [27] Y. Alhassid, G.F. Bertsch, and P. Fanto, Ann. Phys. (N.Y.) **419**, 168233 (2020).  
 [28] Y. Alhassid, G.F. Bertsch, and P. Fanto, Ann. Phys. (N.Y.) **424**, 168381 (2021).  
 [29] P.S. Damle, A.W. Ghosh, and S. Datta, Phys. Rev. B **64**, 201403 (2001).  
 [30] N. Bohr and J.A. Wheeler, Phys. Rev. **56**, 426 (1939).  
 [31] G.F. Bertsch, J. Phys.: Cond. Matt. **3**, 373 (1991).  
 [32] D.L. Hill and J.A. Wheeler, Phys. Rev. **89**, 1102 (1953).  
 [33] See Supplemental Material for the estimates of physical parameters and codes to generate data points in the Figures. It also contains some additional examples.

## Contents

1. Estimates of the physical parameters
2. Compound nucleus limit
3. Codes

## Estimation of physical parameters

*Orbital energy spacing  $d$ .* The single-particle level spacing in the uniform model  $d$  sets the energy scale for the model and does not play any explicit role in the model. However, it is required to determine other energy parameters which are expressed in units of  $d$ . Several estimates of  $d$  for  $^{236}\text{U}$  are given in Table I. The first is based on orbital energies in a deformed Woods-Saxon potential with the parameters given in Ref. [1]; see Table II for the calculated orbital energies.

In more realistic theory, the momentum dependence

$d$ (MeV)	Source
0.45	Woods-Saxon well
0.51	FRLDM [5]
0.33	FGM [6]

TABLE I: Estimated orbital level spacing in  $^{236}\text{U}$ . The first two are from potential models and the last extracted from the Fermi gas formula and measured level densities.

protons			neutrons		
$2K$	$\pi$	$\varepsilon_{K\pi}/d$	$2K$	$\pi$	$\varepsilon_{K\pi}/d$
3	-1	-3.39	5	-1	-4.15
5	-1	-3.80	1	-1	-4.25
5	1	-4.93	7	-1	-4.40
-----			-----		
1	1	-5.43	1	1	-5.07
9	-1	-5.53	5	1	-5.75
3	1	-5.74	5	-1	-5.82

TABLE II: Characteristics of single-particle orbitals in a deformed Woods-Saxon potential corresponding to  $^{236}\text{U}$  at deformation  $(\beta_2, \beta_4) = (0.274, 0.168)$ . Dashed line indicates the Fermi level.

of the potential tends to increase the spacing, but the coupling to many-particle degrees of freedom decreases the spacing of the quasiparticle poles. The combined effect seems to be to somewhat decrease the spacing<sup>1</sup>.

*Level density.* It is important to know the composition of the levels in the compound nucleus to construct mi-

croscopic models that involve those levels. For a concrete example, consider the levels at the neutron threshold energy  $S_n = 6.5$  MeV in  $^{236}\text{U}$ . The predominating configurations at this energy should be  $k$  subblocks at  $k \approx S_n/d$  in the independent quasiparticle approximation. Another approach that is less sensitive to the residual interaction is to estimate the total number of states below  $S_n$  and comparing it to the number obtained by summing the  $N_k$  degeneracies in the  $Q$ -block spectrum. In the  $^{236}\text{U}$  example, the combined level spacing of  $J^\pi = 3^-$  and  $4^-$  is about 0.45 eV at  $S_n$ [10]. At that excitation energy the level density is the same for even and odd parities, and it varies with angular momentum as  $2J + 1$ . The inferred level spacing of  $J^\pi = 0^+$  levels is thus about 7 eV. The accumulative number of levels can be approximated by  $N = \rho T$  where  $T$  is the nuclear temperature, defined as  $T = d \log(\rho(E))/dE$ . A typical estimate for our example is  $T = 0.65$  MeV, giving  $N \approx 1.0 \times 10^8$ . To estimate the level density in the present model, we start with the set of quasiparticle configurations including both parities and all  $K$  values. The resulting  $k$ -blocks have multiplicities that are well fit by the formula

$$N_k \approx \exp(-3.23 + 4.414k^{1/2}). \quad (1)$$

Projection on good parity decreases this by a factor of two. The projection on angular momentum  $J = 0$  is more subtle. The  $J = 0$  states are constructed by projection from  $K = 0$  configurations; other configurations do not contribute. However, there may be two distinct configurations that project to the same  $J = 0$  state. This gives another factor of nearly two reduction in the multiplicity. The remaining task is to estimate the fraction of  $K = 0$  configurations in the unprojected quasiparticle space. The distribution of  $K$  values is approximately Gaussian with a variance given by

$$\langle K^2 \rangle = \langle n_{\text{qp}} \rangle \langle K^2 \rangle_{\text{sp}} \quad (2)$$

where  $\langle n_{\text{qp}} \rangle \approx 8$  is the average number of quasiparticles in the  $k$  block and  $\langle K^2 \rangle_{\text{sp}} \approx 6$  is an average over the orbital  $K$ 's near the Fermi level. Including these projection factors, the integrated number of levels up to  $S_n$  is achieved by including all  $k$ -subblocks up to  $k = 17$  in the entry  $Q$ -block.

*Neutron-proton interaction  $v_{\text{np}}$ .* To set the scale for our neutron-proton interaction parameter  $v_{\text{np}}$  we compare with phenomenological contact interactions that have been used to model nuclear spectra. The matrix element of the neutron-proton interaction is

$$\langle n_1 p_1 | v | n_2 p_2 \rangle = -v_0 I \quad (3)$$

where

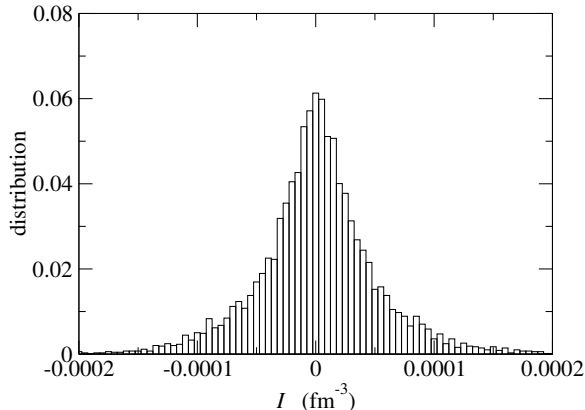
$$I = \int d^3 r \phi_{n_1}^*(\mathbf{r}) \phi_{p_1}^*(\mathbf{r}) \phi_{n_2}(\mathbf{r}) \phi_{p_2}(\mathbf{r}). \quad (4)$$

The parameter  $v_0$  is the strength of the interaction, typically expressed in units of MeV fm<sup>3</sup>. Some values of  $v_0$

<sup>1</sup> We note that in the energy density functional fit including fission data[7] the effective mass in the single-particle Hamiltonian was very close to 1.

Basis of estimate	$v_0$ (MeV fm <sup>3</sup> )	Citation
$G$ -matrix	530	[4]
$sd$ -shell spectra	490	[3]
$\beta$ -decay	395,320	[2]

TABLE III: Estimates of neutron-proton interaction strength.

FIG. 1: Integrals  $I$  in Eq. (4) of orbitals near the Fermi energy.

from the literature are tabulated in Table III. We shall adopt the value  $v_0 = 500$  MeV fm<sup>3</sup> for most of the model calculations.

If the wave functions of the eigenstates approach the compound nucleus limit, the only characteristic we need to know is its mean-square average among the active orbitals. We have calculate the integral Eq. (4) for all the fully off-diagonal matrices of the orbitals within 2 MeV of the Fermi energy. Fig. 1 shows a histogram of their distribution<sup>2</sup>. The variance of the distribution is  $\langle I^2 \rangle^{1/2} = 5.22 \times 10^{-5}$  fm<sup>-3</sup>. Combining this with our estimate of  $v_0$  we find  $(\langle n_1 p_1 | v | n_2 p_2 \rangle^2)^{1/2} = 0.025$  MeV. This implies  $v_{np} \sim 0.05d$  with our estimated single-particle level density.

*Decay widths* Experimentally in the nucleus <sup>236</sup>U at an energy near  $S_n$ , the compound-nucleus gamma decay widths are about 0.040 eV[10]. Such widths are smaller than any of the other energy scales in the reaction. The branching ratio between gamma capture and fission favors fission by about a factor of 3, but  $B_{\text{cap,fiss}}$  has strong fluctuations around that average. There is no direct information about the exit channel decay widths near the scission point. However, for several of the examples in the text we have taken  $\Gamma_{\text{fis}}/\Gamma_{\text{cap}} = 3$ , which would give the observed branching in the (unphysical) compound

nucleus limit.

On the theoretical side, the decay widths of the states in the Hamiltonian enter into the reaction cross sections into two ways, explicitly as a factor in Eq. (5) of the text and implicitly in the Green's function  $(\hat{H} - E)^{-1}$ . If the decay width is smaller than any of the other internal energy scales, one can neglect its effect on the Green's function. It is also the case that the transmission factors depend strongly on the entrance channel widths, but the branching ratios are insensitive. Our reported calculations were carried out in the limit of small entrance channel widths, but realistic ones derived from optical model phenomenology can be easily incorporated, as was done in the MAZAMA code [9].

### Compound nucleus limit.

The concept of the compound nucleus is a major ingredient of the reaction theory for fission of heavy nuclei. From the side of theory, the compound nucleus is characterized by a set of properties derived from Wigner's random matrix model (RME) [11–17], or more specifically the Gaussian orthogonal ensemble (GOE). In our framework, the RME is most closely approached when the space is restricted to a single  $k$ -block. Since the diagonal elements of the Hamiltonian are all the same, the only energy scale relevant to the diagonalization is  $v_{np}$ , the strength of the interaction. However, it is far from guaranteed that the model will satisfy the expected properties because our Hamiltonian is a sparse matrix, unlike the RME. Here we examine the properties of the states in the  $k = 6$  space to show that indeed the model does approach the RME limit. The Hamiltonian matrix has a dimension of  $N_6 = 784$  and there are 29688 off-diagonal matrix elements. To be specific, the interaction strength is taken as  $v_{np} = 0.05d$ .

Properties of the RME that are independent of the basis are the semicircular distribution of eigenvalues and the repulsion between neighboring eigenvalues. The top and the middle panels of Fig. 2 show the eigenvalue distribution and the distribution of the nearest neighbor level spacing compared with the semi-circle formula

$$\rho(E) = \frac{2}{\pi} \frac{N_6}{E_0} \sqrt{1 - \left(\frac{E}{E_0}\right)^2}, \quad (5)$$

and the eigenvalue repulsion formula (i.e., the Wigner distribution),

$$P(x) = \frac{\pi}{2} x e^{-\pi x^2/4} \quad (6)$$

respectively. Here,  $E_0$  in Eq. (5) is a parameter characterizing the width of the eigenvalue distribution, which we take  $E_0 = 0.6d$ , and  $x$  in Eq. (6) is defined as  $x = s/\langle s \rangle$ , where  $s$  is a nearest neighbor level spacing and  $\langle s \rangle$  is its average. The figure indicates that both properties are reasonably well satisfied.

For the problem of fission, the most important property of the compound nucleus is a distribution of

<sup>2</sup> If the orbitals are restricted only to those in TABLE II, the histogram is more structured.

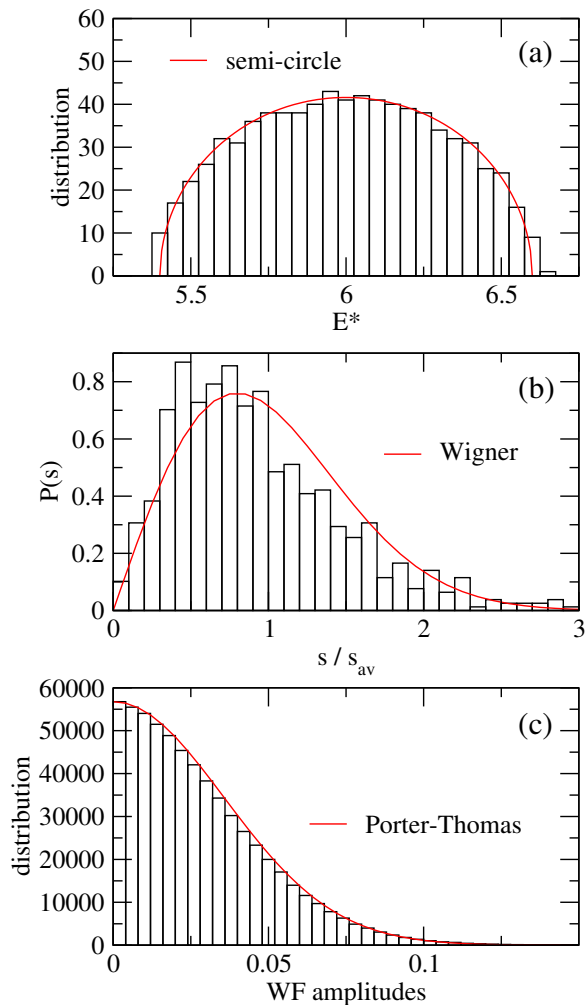


FIG. 2: (a) Eigenvalue spectrum of the neutron-proton interaction with  $v_{np} = 0.05d$  in the  $E^* = 6d$  configuration space. The red solid curve shows the semi-circle distribution, Eq. (5), with  $E_0 = 0.6d$ . (b) The nearest neighbor level spacing distribution compared with the Wigner distribution, Eq. (6). (c) The distribution of wave function amplitudes for all the components of all the eigenstates within the model space. The red solid line shows the expected Gaussian distribution.

decay widths to the individual channels. This should obey the Porter-Thomas distribution if the configuration amplitudes are Gaussian distributed. Taking all the eigenfunctions and configurations of the model space, the bottom panel of Fig. 2 shows the distribution of the wave function amplitudes compared with the Gaussian distribution having the width parameter  $\sigma = N_6^{-1/2}$ . As we see, the distribution agrees well with the Gaussian distribution.

## Codes

Codes to compute selected data points in Figs. 1,3,4, and 5 are provided in the subdirectory `codes`. The Hamiltonian matrices are constructed by Fortran codes `ham*.f`. The subsequent analysis is carried out by Python scripts and shell scripts. The Fortran codes have been compiled and tested with the `gfortran` compiler. The Python scripts are listed below. They compile the necessary Fortran code to generate the Hamiltonians in the ensembles and then calculate the observables according to the formulas in the text.

Fig. 1, histogram: `fig1.py`

Fig. 3, branching ratio at  $f_{od} = 0.5$ : `fig3.py`

Fig. 4, branching ratio at  $\Gamma_{fis} = 0.1$ :

`fig4.py`

Fig. 5,  $B$  at  $N_k = 16$ : `fig5.py`

- 
- [1] A. Bohr and B.R. Mottelson, *Nuclear Structure* (W.A. Benjamin, Reading, MA, 1969), Vol. I.
- [2] K. Yoshida, *Prog. Theor. Exp. Phys.* 113D02 (2013).
- [3] B.A. Brown, *et al.*, *Ann. Phys.* **182** 191 (1988).
- [4] B.W. Bush, G.F. Bertsch and B.A. Brown, *Phys. Rev. C* **45**, 1709 (1992).
- [5] P. Möller, *et al.*, *Atomic Data and Nuclear Data Tables* **59** 185 (1995); private communication (P. Möller).
- [6] A.J. Koning, S. Hilaire, and S. Goriely, *Nucl. Phys. A* **810** 13 (2008).
- [7] M. Kortelainen, *et al.*, *Phys. Rev. C* **85** 024304 (2012).
- [8] G. F. Bertsch, W. Younes, and L. M. Robledo, *Phys. Rev. C* **100**, 024607 (2019).
- [9] G.F. Bertsch and T. Kawano, *Phys. Rev. Lett.* 119 222504 (2017).
- [10] R. Capote, *et al.*, *Nucl. Data Sheets* **110** 3107 (2009).
- [11] T. Guhr and H.A. Weidenmüller, *Ann. Phys. (N.Y.)* **193**, 472 (1989).
- [12] H.A. Weidenmüller and G.E. Mitchell, *Rev. Mod. Phys.* **81**, 539 (2009).
- [13] M.R. Zirnbauer, J.J.M. Verbaarschot, and H.A. Weidenmüller, *Nucl. Phys. A* **411**, 161 (1983).
- [14] S. Drożdż, S. Nishizaki, J. Speth, and J. Wambach, *Phys. Rev. C* **49**, 867 (1994).
- [15] M. Matsuo, T. Døssing, B. Herskind, and S. Frauendorf, *Nucl. Phys. A* **564**, 345 (1993).



- [16] M. Matsuo, T. Døssing, E. Vigezzi, R.A. Broglia, and K. Yoshida, Nucl. Phys. **A617**, 1 (1997).  
Phys. **A620**, 296 (1997).
- [17] M. Matsuo, T. Døssing, E. Vigezzi, and S. Åberg, Nucl.